ELSEVIER

An approach to estimation of near-surface turbulence and CO_2 transfer velocity from remote sensing data

Alexander Soloviev [a,*], Mark Donelan [b], Hans Graber [b], Brian Haus [b], Peter Schlüssel [c]

[a] *Oceanographic Center, NOVA Southeastern University, Dania Beach, Florida 33004, USA*
[b] *Rosenstiel School of Marine and Atmospheric Science, University of Miami, Miami, Florida 33149, USA*
[c] *EUMETSAT, 64295 Darmstadt, Germany*

Abstract

The air–sea CO_2 exchange is primarily determined by the boundary-layer processes in the near-surface layer of the ocean since it is a water-side limited gas. As a consequence, the interfacial component of the CO_2 transfer velocity can be linked to parameters of turbulence in the near-surface layer of the ocean. The development of remote sensing techniques provides a possibility to quantify the dissipation of the turbulent kinetic energy in the near-surface layer of the ocean and the air–sea CO_2 transfer velocity on a global scale. In this work, the dissipation rate of the turbulent kinetic energy in the near-surface layer of the ocean and its patchiness has been linked to the air–sea CO_2 transfer velocity with a boundary-layer type model. Field observations of upper ocean turbulence, laboratory studies, and the direct CO_2 flux measurements are used to validate the model. The model is then forced with the *TOPEX POSEIDON* wind speed and significant wave height to demonstrate its applicability for estimating the distribution of the near-surface turbulence dissipation rate and gas transfer velocity for an extended (decadal) time period. A future version of this remote sensing algorithm will incorporate directional wind/wave data being available from *QUIKSCAT*, a now-cast wave model, and satellite heat fluxes. The inclusion of microwave imagery from the Special Sensor Microwave Imager (*SSM/I*) and the Synthetic Aperture Radar (*SAR*) will provide additional information on the fractional whitecap coverage and sea surface turbulence patchiness.

1. Introduction

The exchange of momentum, energy, and mass across the air–sea interface to a large degree controls the weather, climate, and progress of life in the ocean (Donelan, 1998). The flux of gases like carbon dioxide (CO_2) across the air–sea interface contributes to important processes of the global climate system (Tans et al., 1990; Wanninkhof et al., 1999). On a much smaller scale, the air–sea exchange is determined by the physics of the turbulent boundary-layer and the properties of the free surface. The presence of a free surface dramatically complicates turbulent exchange processes at the air–sea interface. The same free surface serves as an intermediary for ocean remote sensing techniques.

Carbon dioxide is almost infinitely soluble in air; the main difference in gas concentration is therefore on the waterside of the air–sea interface (Bolin, 1960). The

* Corresponding author. Fax: +1 954 2624098.
 E-mail address: soloviev@ocean.nova.edu (A. Soloviev).

formulation for the CO_2 transfer (piston) velocity K is therefore as follows:

$$K = G/\Delta C, \tag{1.1}$$

where G is the air–sea CO_2 flux, and ΔC is the effective air–sea gas concentration difference. Since G is a sum of interfacial (G_{int}) and bubble-mediated (G_b) components, an interfacial $K_{int} = G_{int}/\Delta C$ and a bubble-mediated $K_b = G_b/\Delta C$ gas transfer velocity can separately be defined.

In this paper, we are concerned with the development of remote sensing techniques to quantify the dissipation rate of turbulent kinetic energy in the near-surface layer of the ocean and the air–sea gas transfer. A companion paper (Soloviev, 2007-this issue) considers a renewal type model for parameterizing the interfacial component of the air–sea gas exchange. In this paper, we employ a boundary-layer approach.

The organization of the paper is as follow. Section 2 introduces the boundary-layer concept of air–sea gas exchange, connecting the interfacial component of the gas transfer to the near-surface turbulence dissipation rate. Section 3 outlines an existing theory and a formula for the bubble-mediated component of the gas transfer velocity. In Section 4, the dissipation of the turbulent kinetic energy in the near-surface layer of the ocean is analyzed based on the field and theoretical results. Section 5 proposes a new parameterization for the CO_2 air–sea exchange incorporating dependence on wave age. Sections 6 and 7 are devoted to development of remote sensing algorithms, which may be significantly advanced with the inclusion of surface-wave spectrum and whitecap fraction information. Section 8 is the conclusions.

2. Boundary-layer concept of air–sea gas exchange

In boundary-layer models, the interfacial gas transfer velocity can be parameterized via a relationship of the type proposed by Kitaigorodskii and Donelan (1984) and Dickey et al. (1984):

$$K_{int} \approx b[\varepsilon(0)vSc^{-2}]^{1/4}, \tag{1.2}$$

where b is a dimensionless coefficient, $\varepsilon(0)$ the surface value of the dissipation rate of the turbulent kinetic energy, v is the kinematic viscosity of water, $Sc = v/\mu$ is the Schmidt number, and μ is the kinematic molecular diffusion coefficient of gas.

Relationship (1.2) can alternatively be derived (as in Fairall et al., 2000) from the hypothesis that the thickness of the diffusive molecular sublayer δ_μ is proportional to

the Kolmogorov's internal scale of turbulence for concentration inhomogeneities: $\eta_D = Sc^{-1/2}(v^3/\varepsilon)^{1/4}$, where the thickness of the diffusive sublayer is defined as

$$\delta_\mu = \mu\Delta C/G_{int} = \mu/K_{int}. \tag{1.3}$$

Here $\Delta C = C_w - C_0$ is the effective air–sea gas concentration difference (indices "w" and "0" relate to the bulk and surface values respectively), and G_{int} is the interfacial component of the air–sea gas flux.

Most of the upper ocean is a shear layer, with only a few patches where breaking-wave-generated turbulence dominates. Averaging over turbulence patches has a different effect on the gas transfer velocity compared to the dissipation rate; since, according to Eq. (1.2), the gas transfer velocity is proportional to the quarter power of the dissipation rate. Statistical averaging involves a probability distribution function. The dissipation rate of the turbulent kinetic energy ε obeys a lognormal law (Oakey, 1985):

$$p(\varepsilon) = \frac{1}{(2\pi)^{-1/2}\sigma\varepsilon}\exp\left[-\frac{(\ln\varepsilon - m)^2}{2\sigma^2}\right], t > 0 \tag{1.4}$$

where m is the mean value and σ^2 is the variance for the logarithm of ε, which is treated as a random variable. The expected value of ε^n is then equal to: $\overline{\varepsilon^n} = \exp(mn + n^2\sigma^2/2)$, which results in relationship,

$$\overline{\varepsilon^{1/4}}/(\overline{\varepsilon})^{1/4} = \exp(-3\sigma^2/32). \tag{1.5}$$

Relationship (1.5) in application to formula (1.2) implies that there is a coefficient connecting average dissipation rate and average gas transfer velocity:

$$A_0 = \exp(-3\sigma^2/32), \tag{1.6}$$

which depends on the parameter of lognormal distribution σ.

According to Oakey (1985) and Soloviev and Lukas (2003), for the shear and convective turbulence in the upper ocean mixed layer parameter $\sigma \approx 0.6$, which results in $A_0 \approx 0.97$. For breaking-wave turbulence, σ is expected to be much larger than it is for that generated by shear or convection. Soloviev and Lukas (2003) reported an increase in the value of σ when approaching the wave stirred layer. No statistically significant turbulence measurements directly in the wave-stirred layer can, however, be found in the literature; the value of σ in this layer is virtually unknown. On the other

hand, Woolf (1995) proposed an approximate method to account for the effect of turbulence patchiness on the interfacial gas exchange (which is being used in Section 4 to derive a formula for the weighting coefficients due to turbulence patchiness (Eq. (1.25)).

3. Bubble-mediated component of the air–sea gas exchange

The bubble-mediated gas transport is believed to dominate over the interfacial component under high wind speed conditions. The bubble-mediated component depends on both gas molecular diffusivity and gas solubility (Thorpe and Woolf, 1991). Moderately soluble gases like CO_2 are less dependent on bubble transport than poorly soluble gases (like SF_6).

The bubble-mediated component of the air–sea gas exchange can be parameterized with Woolf's (1997) formula

$$K_b = W \frac{2450}{\beta_0 \left(1 + \frac{1}{(14\beta_0 Sc^{-1/2})^{1/1.2}}\right)^{1.2}} \text{ cm h}^{-1}, \qquad (1.7)$$

where W is the fractional whitecap coverage by stage A whitecaps (defined in Monahan and Lu, 1990), and β_0 is the Ostwald gas solubility.

Formula (1.7) is intended for "clean" bubbles. The bubble-mediated transfer velocity, K_b, is associated largely with a shallow flushing of bubbles, with the exception of gases of extremely low solubility for which the few long-lived bubbles are important (Woolf, 1997). The shallow bubbles, which are less contaminated than deep bubbles, supposedly dominate in the bubble-mediated gas transport of moderately soluble gases like CO_2.

Traditional parameterizations of whitecap coverage are in the form of a power-law dependence on wind speed alone (e.g., Monahan and O'Muircheartaigh, 1980). Zhao and Toba (2001) expressed the whitecap coverage as a regression with respect to a Reynolds-type number R_H:

$$W \approx 4.02 \times 10^{-5} R_H^{0.96}, \qquad (1.8)$$

where $R_H = u_{*a} H_S / \nu_a$, u_{*a} is the friction velocity in air, H_S is the significant wave height, and ν_a is the kinematic air viscosity. The Reynolds-type number R_H is then expressed via the dimensionless parameter

$$R_B = A_w u_{*a}^3 / (g\nu_a), \qquad (1.9)$$

using the Toba (1972) "3/2-power" law linking the non-dimensional significant wave-height and period via relationship:

$$R_H = B(2\pi/1.05)^{3/2} A_w^{1/2} R_B, \qquad (1.10)$$

where $B = 0.062 \pm 0.012$ is an empirical constant; A_w is the wave age defined as $A_w = g/(u_{*a}\omega_p)$, where ω_p is the peak frequency in the wind-wave spectrum.

From Toba's (1972) law it is also possible to express the wave age A_w via the significant wave height H_S and friction velocity u_* as:

$$A_w = \frac{1}{2\pi} \left(\frac{gH_S\rho_a}{0.062\rho u_*^2}\right)^{2/3}. \qquad (1.11)$$

where $u_* = (\rho_a/\rho)^{1/2} u_{*a}$ is the friction velocity in water.

Estimation of gas transfer velocity from satellites based on both wind speed and surface-wave information is potentially more accurate than that based on wind speed alone. Zhao et al. (2003) and Woolf (2005) proposed to use R_B as a breaking-wave parameter and regression (1.8) to obtain a sea-state dependent parameterization of the bubble-mediated component of gas transfer velocity. The analysis presented in the next two sections has allowed us to incorporate the stage of wind-wave development into the parameterization of the interfacial component of gas transfer velocity.

4. Dissipation rate of turbulent kinetic energy in the near-surface layer of the ocean

The dissipation rate of the turbulent kinetic energy in the surface layer of the ocean can be represented as a sum of convection ε_c, shear ε_u, and wave ε_w terms:

$$\varepsilon = \varepsilon_c + \varepsilon_u + \varepsilon_w. \qquad (1.12)$$

Formula (1.2) linking K_{int} and ε includes the surface value of the dissipation rate $\varepsilon(0)$, which is expressed from Eq. (1.12) via the surface values: $\varepsilon(0)$, $\varepsilon_u(0)$, and $\varepsilon_w(0)$. Below we consider convective, shear, and wave breaking generated turbulence.

4.1. Convective

The convective dissipation term is represented by a classic formula:

$$\varepsilon_c(0) = -\frac{\alpha_T g Q_0}{c_p \rho}, \qquad (1.13)$$

where α_T is the thermal expansion coefficient (negative in this notation), g is the acceleration due to gravity, c_p and ρ are the specific heat and density of water, and Q_0 is the virtual surface heat flux (positive when directed from the ocean to atmosphere). The virtual heat flux is defined according to Fairall et al. (2000) as $Q_0 = Q_E + Q_T + I_L + \frac{\beta_S S_0 c_p}{-\alpha_T L} Q_E$, where Q_E and Q_T are the latent and sensible heat fluxes, I_L is the net longwave irradiance, β_S is the salinity contraction coefficient, S_0 is the surface salinity, and L is the latent heat of water evaporation.

4.2. Shear

The surface value of the shear term is defined as

$$\varepsilon_u(0) \approx \frac{(\tau_t/\rho)^{3/2}}{\kappa \delta_v}, \tag{1.14}$$

where κ is the von Karman constant ($\kappa = 0.4$), δ_v is the effective thickness of the aqueous viscous sublayer, and τ_t is the tangential component of wind stress. According to Soloviev and Schlüssel (1996), the connection between tangential τ_t and total τ_0 wind stress can be parameterized as follows:

$$\tau_t \approx \frac{\tau_0}{1 + Ke/Ke_{cr}}, \tag{1.15}$$

where Ke is the Keulegan number ($Ke = u_*^3/(g\nu)$), u_* is the friction velocity in water, and g is the acceleration due to gravity. Following Soloviev and Lukas (2006) the critical Keulegan number is:

$$Ke_{cr} \approx \frac{\nu_a}{\nu}\left(\frac{\rho_a}{\rho}\right)^{3/2}\frac{R_{Bcr}}{A_w}, \tag{1.16}$$

where ρ_a is the air density, ρ is the water density, and $R_{Bcr} \approx 10^3$ is the critical value of the R_B number (see Eq. (1.9) for definition). The thickness of the aqueous viscous sublayer entering Eq. (1.14) is as follows:

$$\delta_v = c_1\nu/(\tau_t/\rho)^{1/2}, \tag{1.17}$$

where c_1 is a dimensionless constant. The surface value of the shear related turbulence dissipation is then formulated as follows:

$$\varepsilon_u(0) = \frac{(\tau_t/\rho)^2}{\nu} \approx \frac{u_*^4}{\kappa c_1 \nu (1 + Ke/Ke_{cr})^2} \tag{1.18}$$

4.3. Wave breaking

The breaking-wave dissipation rate of the turbulent kinetic energy in the near-surface layer of the ocean has

been the subject of many discussions in the oceanographic literature (Kitaigorodskii et al., 1983; Soloviev et al., 1988; Terray et al., 1996; and others). The Craig and Banner (1994) eddy–viscosity model, which employs a level "2-1/2" turbulence closure scheme of Mellor and Yamada (1982), has demonstrated reasonable agreement with the extensive near-surface data set obtained during TOGA COARE (Soloviev and Lukas, 2003). According to the Soloviev and Lukas (2003), the dissipation rate of the breaking-wave-generated turbulence can be described by the following formula:

$$\varepsilon_w(0) = \alpha_w \left(\frac{3}{BS_q}\right)^{1/2}\frac{F_0}{\kappa z_0}, \tag{1.19}$$

where F_0 is the flux of the turbulent kinetic energy to waves from wind, z_0 is the surface roughness scale (from the water side); B and S_q are the dimensionless constants ($B = 16.6$, $S_q = 0.2$). Parameterization for z_0 is of the Terray et al. (1996) type,

$$z_0 = c_T H_S, \tag{1.20}$$

where C_T is a dimensionless constant.

The flux F_0 is parameterized as

$$F_0 = \alpha_w \rho (\tau_w/\rho)^{3/2} \tag{1.21}$$

where α_w is a function of wave age, which for developed seas ($A_w > 12$) is approximately constant and equal to $\alpha_w \approx 100$; τ_w is the wave-induced component of wind stress. From Eq. (1.15) it follows that

$$\tau_w = \tau_0 - \tau_t \approx \frac{Ke/Ke_{cr}}{1 + Ke/Ke_{cr}}\tau_0. \tag{1.22}$$

The surface value of the breaking-wave turbulence generation is then determined from Eqs. (1.15), (1.19) and (1.20) as:

$$\begin{aligned}\varepsilon_w(0) = \alpha_w &\left(\frac{3}{BS_q}\right)^{1/2}\\ &\times \frac{(Ke/Ke_{cr})^{3/2}}{(1 + Ke/Ke_{cr})^{3/2}}\frac{u_* g}{0.062\kappa c_T (2\pi A_w)^{3/2}}\frac{\rho_a}{\rho}.\end{aligned} \tag{1.23}$$

Turbulence measurements in the near-surface layer of the open ocean are rare. This kind of measurement is complicated by the presence of surface-wave disturbances and some other factors. The velocity scale of turbulent fluctuations in the near-surface layer of the ocean is about
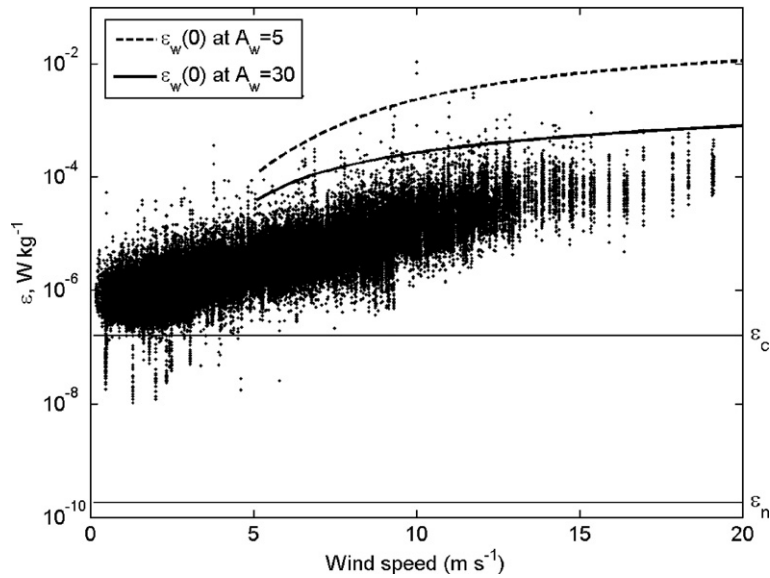
Fig. 1. Each point represents a 10-min average (no sorting by depth in this graph) of the dissipation rate of TKE from the bow sensors versus wind speed, U_{15}, at 15 m height, during a month-long TOGA COARE cruise of the R/V *Moana Wave* (Soloviev and Lukas, 2003). The equivalent electronic noise of the sensor is indicated as a horizontal line $\varepsilon_n = 1.8 \times 10^{-10}$ W kg^{-1}; the level of dissipation rate due to free convection at surface heat flux $Q_0 = 200$ W m^{-2}, as horizontal line $\varepsilon_c = 1.3 \times 10^{-7}$ W kg^{-1}. Theoretical surface dissipation rates due to wave-breaking are shown for two values of the wave age, A_w.

1 cm s^{-1}, while the typical surface-wave orbital velocity is of ~ 1 m s^{-1}. (This means that the disturbance is about 100 times stronger than the useful signal.) The presence of such exceptionally strong disturbances from the surface-wave orbital velocities imposes special requirements on the measurement techniques and sensors for observation of near-surface turbulence.

An extended open-ocean data set on near-surface turbulence has recently been reported by Soloviev and Lukas (2003). These data were obtained during the month-long COARE Enhanced Monitoring cruise EQ-3 using a microstructure sensor system mounted on the bow of the vessel. The experimental techniques provided an effective separation between the surface waves and turbulence, using the difference in spatial scales of the energy containing surface waves and small-scale turbulence. The dissipation rates were obtained within a wide range of wind speeds (up to 19 m s^{-1}).

Fig. 1 shows the dissipation rates collected by Soloviev and Lukas (2003) during a month long COARE cruise as a function of wind speed. The data in Fig. 1 are not sorted by depth. The theoretical values of the surface dissipation rates due to wave breaking calculated according to Eq. (1.23) provide the upper limit for ε, which appears to be consistent with the data. Note that Soloviev and Lukas (2003) had to remove the data affected by air-bubble disturbances, which explains a relatively low number of experimental points close to the sea surface, especially at high wind speeds.

Convection as a source of TKE in the near-surface layer of the ocean is also schematically shown in Fig. 1. Its contribution to the turbulent mixing under moderate and high wind speed conditions is negligible. The convection as a source of the near-surface mixing can, however, become important under very low wind speed conditions (though it may be suppressed due to solar warming).

In Fig. 2, the vertical profiles of the near-surface dissipation rate are compared to several models of near-surface turbulence. The Craig and Banner (1994) model, which results in equation for calculation of the surface dissipation rate (Eq. (1.23)), is in a reasonably good agreement with the dissipation data.

5. Parameterization of the air–sea CO_2 exchange

Assembling Eqs. (1.2), (1.13), (1.18), and (1.23) into a single expression leads to the following parameterization formula for the interfacial gas transfer velocity:

$$K_{int} = bSc^{-1/2} \left[\begin{array}{c} -\dfrac{A_c^4 \alpha_T g Q_0 \nu}{c_p \rho} + \dfrac{A_u^4 u_*^4}{\kappa c_1 (1 + Ke/Ke_{cr})^2} \\[2ex] + A_p^4 \alpha_w \left(\dfrac{3}{BS_q} \right)^{1/2} \dfrac{(Ke/Ke_{cr})^{3/2}}{(1 + Ke/Ke_{cr})^{3/2}} \dfrac{u_* g \nu}{0.062 \kappa c_T (2\pi A_w)^{3/2}} \dfrac{\rho_a}{\rho} \end{array} \right]^{1/4}.$$

$$(1.24)$$

where A_c, A_u, and A_p are the weighting coefficients due to turbulence patchiness of convection, shear, and breaking-wave generated turbulence, respectively.
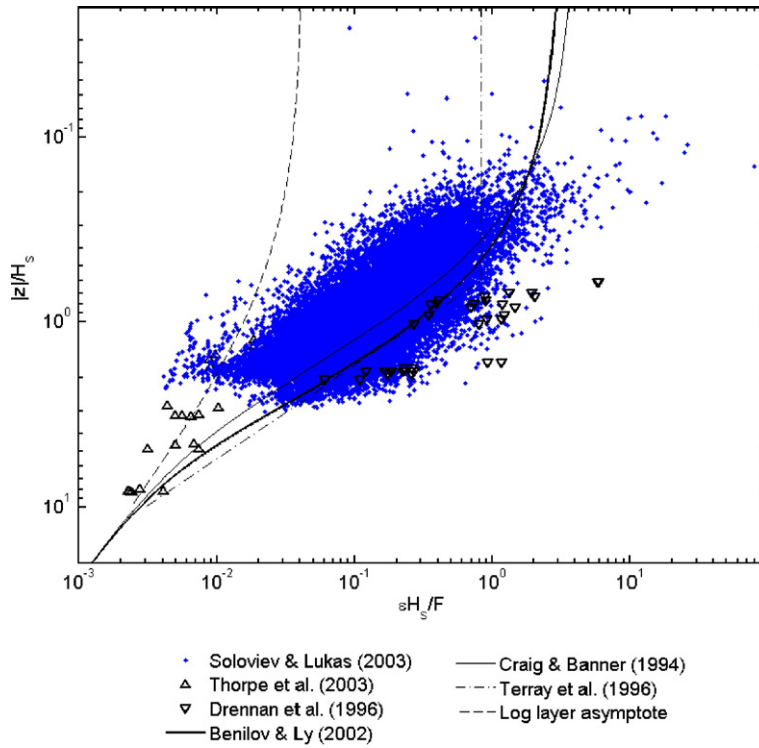
Fig. 2. Normalized dissipation rate $\varepsilon H_S/F_0$ versus dimensionless depth $|z|/H_S$ according to field (open ocean) and theoretical results. Here: ε is the dissipation rate of the turbulent kinetic energy, F_0 the flux of the kinetic energy from wind to waves, and H_S the significant wave height. Dots, and upward and downward looking triangles are respectively the measurements of Soloviev and Lukas (2003, 2006), Thorpe et al. (2003), and Drennan et al. (1996) in the wind speed range is from 7 m s^{-1} to 19 m s^{-1}. The Craig and Banner (1994) model (thin continuous curve) is calculated with surface roughness from waterside parameterized as $z_0 = 0.6\,H_S$; the Benilov and Ly (2002) model (thick continuous line) is for $H_{w-s}/H_S = 0.4$, where H_{w-s} is the effective depth of the wave-stirred layer.

Assuming that $A_c = A_u = A_0$, while according to Eq. (1.6): $A_0 \approx 0.97$. From the Woolf (1995) model of breaking-wave-generated turbulence it follows that:

$$A_p = \frac{8}{5}\left(\frac{11}{2}\right)^{1/4} W\left(\frac{1}{W^{1/4}} - 1\right) \approx 2.45 W\left(\frac{1}{W^{1/4}} - 1\right), \quad (1.25)$$

where the whitecap coverage, W, can be parameterized via Eqs. (1.8), (1.9), (1.10).

Taking into account Eq. (1.25) formula (1.24) transforms as follows:

$$K_{int} = \frac{A_0 u_*}{Sc^{1/2} \Lambda_0} \frac{(1 - a_0^3 \Lambda_0^4 Rf_0)^{1/4}}{(1 + Ke/Ke_{cr})^{1/2}} f(Rf_0, Ke, A_w), \quad (1.26)$$

where

$$f = \left[1 + \frac{39.5 W}{(2\pi)^{3/2} A_0^4}\left(\frac{1}{W^{1/4}} - 1\right)\left(\frac{3}{BS_q}\right)^{1/2} \left(\frac{\rho v^2 Ke}{\rho_a v_a^2 Ke_{cr}}\right)^{1/2} \frac{\alpha_w a_0^3 \Lambda_0^4 (1 + Ke/Ke_{cr})^{1/2}}{(1 - a_0^3 \Lambda_0^4 Rf_0)\kappa c_T A_w^{1/2} R_{Bcr}} \right]^{1/4}, \quad (1.27)$$

Sc is the Schmidt number (defined in Section 2), $Rf_0 = \frac{\alpha_T g Q_0 v}{c_p \rho (\tau_t/\rho)^2}$ is the surface Richardson number, Ke is the Keulegan number (defined in Section 4), and A_w is the wave age (defined in Section 3). Critical Keulegan number Ke_{cr} is related to the wave age A_w according to Eq. (1.16).

In Eqs. (1.26) and (1.27), the principle independent variables that determine the case are the friction velocity u_* and the virtual heat flux Q_0. Parameters v, v_a, ρ, and ρ_a are the material constants (water and air viscosities and densities, respectively); κ, B and S_q are the turbulence constants (defined in Section 4). The empirical coefficients that are to be determined from other experiments are a_0, A_0, c_T, α_w, and Λ_0.

In Eqs. (1.26) and (1.27) the dimensionless constant b entering Eq. (1.2) has been replaced for convenience by $b = a_0^{3/4}$, while the dimensionless constant c_1 has been replaced by $c_1 = a_0^3 \Lambda_0^4 / \kappa$. The constant a_0 is defined in such a way that it is identical to that entering Katsaros's et al. (1977) formula for free convection regime, which can be determined from laboratory experiments.
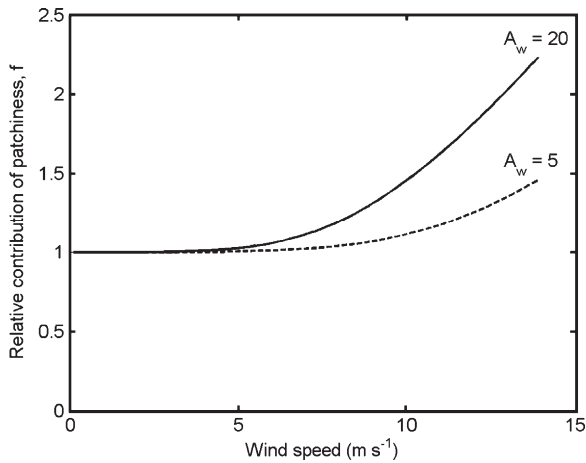
Fig. 3. Factor f characterizing relative distribution of patchiness as a function of wind speed and wave age A_w.

Note that relationship (1.26) resembles the formula derived from a boundary-layer model (Fairall et al., 2000) and from modeling surface renewals (Soloviev and Schlüssel, 1994). The difference is in a factor $f(Rf_0, Ke, A_w)$, which describes the effect of turbulent patches. The new element is also the dependence of the gas transfer parameterization on wave age.

The surface renewal theory (Soloviev and Schlüssel, 1994; Soloviev, 2007-this issue) allows derivation of a coupled set of parameterizations for the velocity difference in the viscous sublayer, the temperature difference across the thermal sublayer (cool skin), and the interfacial gas transfer velocity (for water-side limited gases). Based on the renewal concept Soloviev (2007-this issue) derived numerical values of coefficients A_0 and Λ_0 using data of laboratory experiments of Garbe et al. (2001) and Zhang and Harrison (2004) respectively.

Taking the values of constants $a_0 = 0.25$, $A_0 = 0.9$, and $\Lambda_0 = 7.4$ from Soloviev (2007-this issue) and $c_T = 0.6$ from turbulence results of Soloviev and Lukas (2003), factor f is shown in Fig. 3 as a function of wind speed and wave age. According to this graph, the patchiness is important for wind speeds exceeding approximately 5 m s^{-1}. Developed seas ($A_w = 20$) are the subject to stronger effect of patchiness then young seas ($A_w = 5$).

The model constant Λ_0 can be linked to the coefficient λ introduced by Saunders (1967) in the following way (we here ignore dependence on the surface Richardson number Rf_0, which is important under very low wind speed conditions):

$$\lambda \approx Pr^{-1/2} \Lambda_0 (1 + Ke/Ke_{cr})^{1/2}/f. \tag{1.28}$$

Wind waves generated in a laboratory experiment are characterized by short fetches and thus relatively small A_w; as a result, for not very strong winds $Ke \ll Ke_{cr}$, $f \approx 1$, and Eq. (1.28) reduces to:

$$\lambda \approx Pr^{-1/2} \Lambda_0. \tag{1.29}$$

With the determination of $\Lambda_0 \approx 7.4$ and Prandtl number $Pr \approx 7.5$ (at atmospheric pressure, 20 °C temperature, and 35 ppt salinity), from relation (1.29) it follows that $\lambda \approx 2.7$, which is much lower than previously accepted values but close to the direct measurement of the cool skin with a micro-wire sensor made in the RSMAS Air–Sea Interaction Salt Water Tank Facility (ASIST) by Ward and Donelan (2006). For developed waves, Eq. (1.28) should be used instead of Eq. (1.29), which results in much larger values of Saunder's coefficient λ, usually observed during radiometric measurements in the open ocean.

The parameterization for the air–sea gas exchange is finally represented by a sum of interfacial (Eq. (1.26)) and bubble-mediated (Eq. (1.7)) components:

$$K = K_{int} + K_b. \tag{1.30}$$

Fig. 4 compares parameterization (1.30) with the results of direct, eddy-correlation measurements of the CO_2 air–sea flux during *GasEx-2001* (Hare et al., 2004). The resultant curve demonstrated in Fig. 4 suggests a good agreement between model and observations encouraging further exploration of the applicability of boundary-layer models for parameterization of the interfacial air–sea gas transfer velocity.
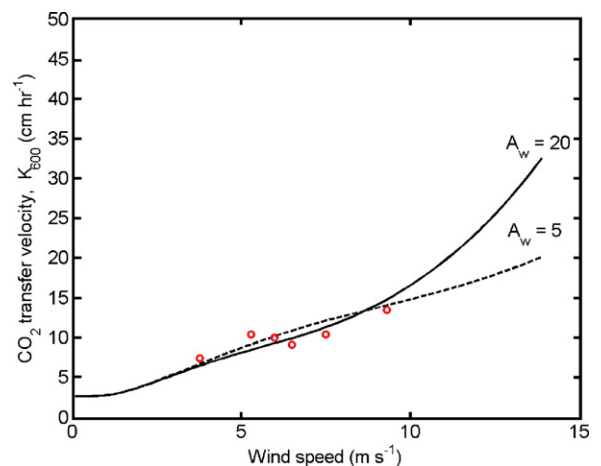

Fig. 4. Gas-transfer parameterization (1.30) for CO_2 at two wave ages in comparison with the direct air–sea CO_2 flux measurements during *GasEx-2001* data by Hare et al. (2004).
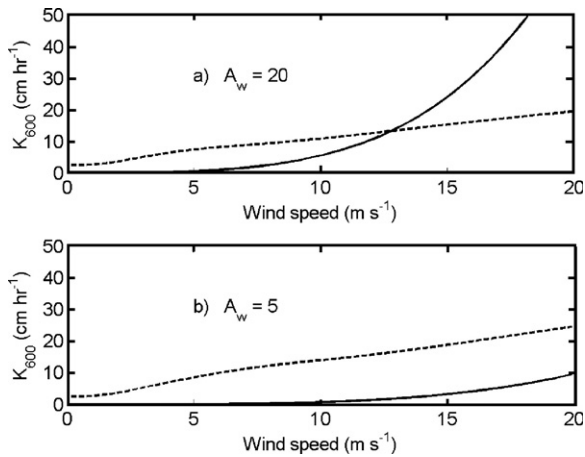
Fig. 5. Interfacial (dashed) and bubble-mediated (continuous) components of the CO_2 transfer velocity parameterization plotted separately for (a) old ($A_w=20$) and (b) young ($A_w=5$) waves.

Surprisingly, in the wind speed range up to approximately 10 m s^{-1} the theoretical gas transfer velocity appears to be insensitive to the wave age. This is explained by the fact that the bubble mediated and interfacial components of the gas transfer depend on the stage of the wave development in an opposite way, thus compensating each other within the range of moderate wind speed conditions. Under high wind speed conditions when the bubble-mediated component significantly exceeds the interfacial component, the parameterization exhibits higher values of the gas transfer velocity for old ($A_w=20$) than young ($A_w=5$) seas.

This fact is also illustrated in Fig. 5 showing separately the interfacial and bubble mediated components of the CO_2 gas transfer parameterization. For old waves, the bubble-mediated component of the gas transfer velocity dominates over the interfacial component for wind speeds exceeding 10–15 m s^{-1}. For young waves, the bubble-mediated component of the gas transfer velocity is much smaller than the interfacial component up to very high wind speeds.

In Fig. 6, gas-transfer parameterization (1.30) plotted for two extreme wave ages $A_w=5$ (very young waves) and $A_w=40$ (fully-developed wind waves) is shown in comparison with other gas transfer velocity relationships. Note that none of the other gas transfer parameterizations shown in Fig. 6 take into account wave age. Under high wind speed conditions most of the other known parameterizations (such as Liss and Merlivat, 1986; Wannikhof, 1992; Nightingale et al., 2000) appear to be within the range described by formula (1.30) between conditions of very young to full-developed wind waves. An exception is the Wanninkhof and McGillis (1999) formula, which predicts somewhat

higher values of the gas transfer velocity. Note that the Wanninkhof and McGillis (1999) parameterization is an interpolation of the direct CO_2 flux measurements during GasEx-1998.

6. Remote sensing approach

During TOGA COARE, Soloviev and Lukas (2003) reported good agreement between the TOPEX/POSEI-DON satellite (Callahan et al., 1994) and shipboard observations of the significant wave height and wind speed. For demonstration purposes, the eddy–viscosity model of near-surface turbulence described in Section 4 is forced with the significant wave height and wind speed obtained from the TOPEX/POSEIDON satellite (Fig. 7). The surface value of the dissipation rate of the turbulent kinetic energy due to wave breaking and the CO_2 transfer velocity calculated from Eqs. (1.23) and (1.30) are shown in Fig. 8. The histogram of CO_2 transfer velocities reveals occasional extremely high values of the gas transfer coefficient, reaching 140 cm h^{-1}.

Under moderate and high wind speed conditions, $\varepsilon(0) \sim U_a^3/H_S$ and $K \sim U_a^{3/4}H_S^{1/4}$ where U_a is the wind speed and H_S is the significant wave height. The error in the determination of U_a and H_S from satellite data translates into the relative error estimates:

$$\Delta\varepsilon/\varepsilon(0) = [(3\Delta U_a/U_a)^2 + (\Delta H_S/H_S)^2]^{1/2},$$

$$\Delta K/K = [(3\Delta U_a/U_a)^2 + (\Delta H_S/H_S)^2]^{1/2}/4.$$

The commonly accepted RMS error estimate for satellite derived wind speeds is $\Delta U_a \approx 2$ m s^{-1}. Callahan
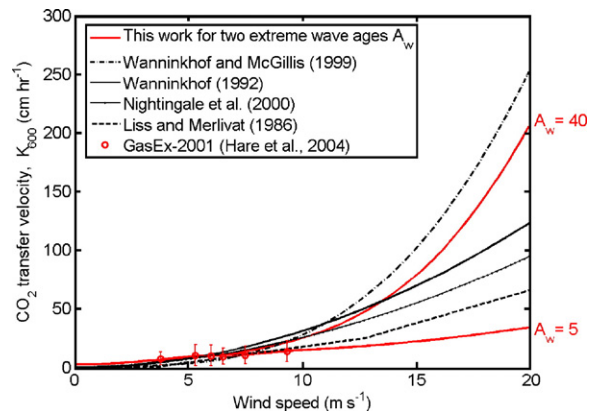

Fig. 6. Gas-transfer parameterization (1.30) for CO_2 at two wave ages A_w in comparison with other gas transfer velocity relationships (shown with confidence intervals here).
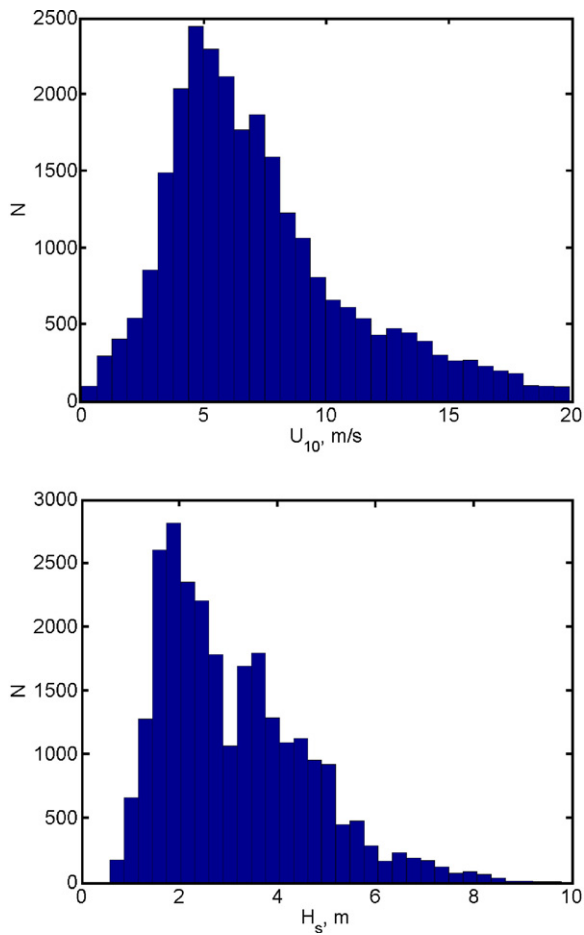
Fig. 7. Wind speed and significant wave height from the TOPEX POSEIDON satellite: September 26, 1992– November 26, 1995, 30° N, 41° W.

Under low wind speed conditions, the upper ocean turbulence and air–sea gas exchange may depend on air–sea heat fluxes. The air–sea heat fluxes can be estimated from satellite data (Schlüssel et al., 1995; Schulz et al., 1996; Benthamy et al., 2001; Johnes et al., 2001; Pinker et al., 2001; Benthamy et al., 2003; Jo et al., 2004; Pan et al., 2004). Space-borne infrared and microwave imagery from the Advanced Very High Resolution Radiometer and from the Special Sensor Microwave/Imager has been used to retrieve boundary-layer parameters for the time period corresponding to GasEx-1998 (Schlüssel and Soloviev, 2001; Soloviev and Schlüssel, 2002). These are the sea surface temperature, surface friction velocity, low-level atmospheric humidity, near-surface stability, and the atmospheric back radiation. These parameters are used to calculate energy and momentum fluxes which in turn are used together with surface renewal modeling to parameterize the temperature difference across the thermal molecular boundary-layer of the upper ocean and the air–sea gas exchange transfer
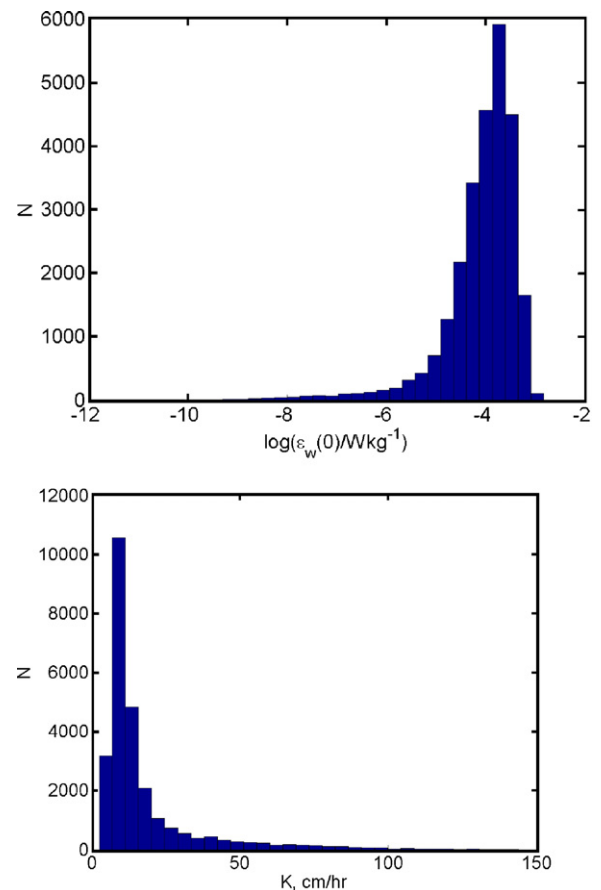
Fig. 8. Turbulence and gas transfer velocity estimates from the *TOPEX/POSEIDON* satellite: September 26, 1992– November 26, 1995, 30° N, 41° W.

et al. (1994) found that in the range of SWH between 1.0 and 3.5 m (this range covers the majority of SWH values encountered in the ocean), the RMS disagreement between the TOPEX altimeter and buoy SWH was $\Delta H_S \approx 0.17$ m with the mean offset of -0.03 m. The above error estimates suggest that the error in wind speed will dominate, which results in $\Delta \varepsilon / \varepsilon(0) \approx 3 \Delta U_a / U_a$, and $\Delta K / K = 3/4 \ \Delta U_a / U_a$. Intensive surface-wave breaking is observed at $U_a > 6$ m s^{-1}, which corresponds to $\Delta \varepsilon / \varepsilon(0) < 1$ and $\Delta K / K < 0.25$. Due to the strong intermittence of turbulence, the dissipation rate of turbulent kinetic energy is known within a factor of 2 (Oakey, 1985). Thus the error in gas transfer velocity is about 25%, which is the usual accuracy of the bulk flux algorithms. For $U_a > 6$ m/s (moderate and high wind speed conditions), the error in the wind speed measurement from satellites therefore is not the main limiting factor of the remote sensing techniques.

velocity. According to Benthamy et al. (2003), and Jo et al. (2004) the relative error in remote sensing of the sensible and latent heat fluxes is normally 25–30%, which translates in approximately the same error in ε and an even smaller error in K.

Surface films can dramatically reduce the air–sea gas exchange through modification of the capillary wave field (Frew et al., 1995). According to Bock et al. (1999) and Jaehne et al. (1987) the gas transfer velocity shows a correlation with the mean square slope regardless of the surfactant concentrations. Due to the fact that the remotely sensed wind speed (like that shown in Fig. 7) is determined from the mean square slopes, these wind velocities may have in effect been adjusted for the influence of surface films. Consequently, the use of such adjusted wind velocities in estimating the gas transfer velocity substantially would eliminate the need to make further adjustments for the presence of surface films. At this point, unfortunately, there are no sufficient data to confirm this statement for open ocean conditions.

7. Advanced remote sensing algorithm

Breaking is the main factor in wave energy dissipation (Komen et al., 1994). Terray et al. (1996) and Gemmrich and Farmer (1999) suggest that the energy transfer from the wind to the wave field is the driving parameter for wave breaking. In fact, only a small fraction of the wave-induced stress ($\sim$5%) is radiated in the wave momentum flux. The vast majority of the wave-induced stress is continuously lost by waves as they dissipate, essentially due to wave breaking (Donelan, 1998; Rascle et al., in press).

The flux of kinetic energy to waves from wind can be determined as the integral of the growth rate, β, over the wave spectrum, where β is the e-folding scale for the temporal growth of wave energy in the absence of nonlinear interactions and dissipation (Terray et al., 1996). Then,

$$F = g \int \frac{\partial S_\eta}{\partial t} \mathrm{d}\omega \mathrm{d}\theta = g \int \beta S_\eta \mathrm{d}\omega \mathrm{d}\theta \qquad (1.31)$$

where $S_\eta(\omega,\theta)$ is the frequency-direction spectrum of the surface waves. A formulation due to Donelan and Pierson (1987) relates β at each frequency to the wind speed as

$$\frac{\beta}{\omega} = 0.194 \frac{\rho_a}{\rho_w} \left(\frac{U_{\pi/k}\cos\theta}{c(k)} - 1 \right) \left| \frac{U_{\pi/k}\cos\theta}{c(k)} - 1 \right| \qquad (1.32)$$

where the wind speed at one half wavelength (π/k) is taken to be the relevant forcing parameter for a component of wavenumber, k, and $c(k)$ is the phase speed.

The simplified version of the boundary condition for the wind energy input in the form Eq. (1.21) may not work well in some cases. A more advanced version of the eddy–viscosity model of near-surface turbulence may utilize directional parameters of the wind and wave fields using approach Eqs. (1.31) and (1.32). In particular, QUIKSCAT may provide wind velocity vectors; while, a now-cast global wave-field model may provide the wave directional spectrum. SAR images may give additional information about the long wave part of the wave spectrum, which can be useful in some cases.

Spaceborne Ku-band scatterometry have generally provided accurate surface wind vectors to the range of wind speeds over which the global operational network of ocean data buoys can be considered to provide accurate and unbiased wind speed measurements. However, recently Donnelly et al. (1999) demonstrated that useful sensitivity of Ku-band scatterometry exists to wind speeds of at least 40 m s^{-1} by the analysis aircraft flight data in hurricanes for regions free from rain. As shown by Atlas et al. (1999), SCAT data can also have a significant impact on numerical weather prediction if the 10-meter winds in extratropical cyclones are assimilated in a way which extends their influence to higher levels in the atmosphere and which allows more accurate retrieval of sounder data through an improved surface pressure field. We can expect the impacts to be even greater when SCAT retrievals that cover the range of 20–40 m s^{-1} are used. Most current numerical weather prediction models assimilate scatterometer and SSMI winds and then force wave prediction models. Ocean wave models like WAM and WAVEWATCH generate directional wave spectra globally. Datasets of the directional wave spectra will be obtained either from the FNMOC global forecast system or from NOAA's NCEP model predictions.

The bubble-mediated gas transfer velocity can be determined based on Woolf's formula (1.7) and the fractional whitecap coverage measures from satellite can be derived from Monahan et al., 1983 model as a function of wind speed using both scatterometer and passive microwave wind speeds. To estimate the whitecap coverage contribution from the SSMI brightness temperature the proposed relationship by Wang et al. (1995) will be used,

$$W_B^h = 7.88 \times 10^{-3} T_h(°K) - 0.893$$

$$W_B^v = 8.96 \times 10^{-3} T_v(°K) - 1.528$$

where W_B^h and W_B^v are the whitecap coverage estimated from the horizontal T_h and vertical T_v polarized sea

surface brightness temperature, respectively. While most whitecaps occur during active generation of waves, there are also conditions such as low wind and swell that dominate in the tropical oceans when whitecaps are present. Intercomparisons of the white-cap coverage determined from the scatterometer wind vectors and the brightness temperature and wind speeds of passive microwave radiometer measurements will lead to better estimates of the whitecap coverage for different sea state and wind conditions. Higher resolution brightness temperature and polarimetry from WindSAT has become available and will allow for more accurate estimates of fractional whitecap coverage.

8. Conclusions

The boundary-layer model described in this work is based on the physics of turbulent boundary-layer near a free interface. In contrast to renewal models (Soloviev and Schluessel, 1994; Soloviev, 2007-this issue) the boundary-layer model does not explicitly include intermittency of exchange processes near the surface. Instead, it identifies the connection between the interfacial gas transfer velocity and the dissipation of the turbulent kinetic energy directly following Kitaigorodskii and Donelan (1984) and Dickey et al. (1984) or indirectly via the Kolmogorov's internal scale of turbulence (Fairall et al., 2000). Since both the renewal and the boundary-layer model are based on equivalent physical principles of the boundary-layer turbulence, they ultimately lead to quite similar final parameterizations.

Though it is still a long way for producing robust parameterization scheme for air–sea gas exchange providing global coverage (i.e., consistent with remote sensing methods), there has been significant progress in this direction during the last decade. An advantage of physically based versus empirical parameterizations is that the former can potentially provide global coverage, while the latter will require adjustment of their empirical coefficients for specific climatic regions, seasons, and, perhaps, even for single weather events. The main uncertainties remain in the effect of surface films and bubbles on the air–sea exchange as well as on the near-surface turbulence.

References

Atlas, R., Bloom, S.C., Hoffman, R.N., Brin, E., Ardizone, J., Terry, J., Bungato, D., Jusem, J., 1999. Geophysical validation of NSCAT winds using atmospheric data and analyses. EOS, Transit. 78 (23), 11405–11424.

Benilov, A.Y., Ly, L.N., 2002. Modeling of surface waves breaking effects in the ocean upper layer. Math. Comput. Model. 35, 191–213.

Benthamy, A., Katsaros, K.B., Mestas-Nunez, A.M., Forde, E.B., Drennan, W.M., Roquet, H., 2001. Latent heat fluxes over the ocean from merged satellite data. WCRP/SCOR Workshop on Intercomparison and Validation of Ocean-Atmosphere Flux Fields, May 21–24, 2001, Bolger Center, Potomac, MD, pp. 10–13.

Benthamy, A., Katsaros, K.B., Mestas-Nunez, A.M., Drennan, W.M., Forde, E.B., Roquet, H., 2003. Satellite estimates of wind speed and latent heat flux over the global oceans. J. Climate 16, 637–656.

Bock, E.J., Hara, T., Frew, N.M., McGillis, W.R., 1999. Relationship between air–sea gas transfer and short wind waves. J. Geophys. Res. 104, 25,821–25,831.

Bolin, B., 1960. On the exchange of carbon dioxide between atmosphere and sea. Tellus 12 (3), 274–281.

Callahan, P.S., Morris, C.S., Hsiao, V., 1994. Comparison of TOPEX/POSEIDON $\sigma°$ and significant wave height distributions to Geosat. J. Geophys. Res. 99, 25,015–25,024.

Craig, P.D., Banner, M.L., 1994. Modeling wave-enhanced turbulence in the ocean surface layer. J. Phys. Oceanogr. 24, 2546–2559.

Dickey, T.D., Hartman, B., Hammond, D., Hurst, E., 1984. A laboratory technique for investigating the relationship between gas transfer and fluid turbulence. In: Brutsaert, W., Girka, G.H. (Eds.), Gas Transfer at Water Surfaces, pp. 93–100.

Donelan, M.A., 1998. Air–water exchange processes. Physical Processes in Lakes and Oceans. Coastal and Estuarine Studies, vol. 54, pp. 19–36.

Donelan, M.A., Pierson Jr., W.J., 1987. Radar scattering and equilibrium ranges in wind-generated waves with application to satterometry. J. Geophys. Res. 92, 4971–5029.

Donnelly, W.J., Carswell, J.R., McIntosh, R.E., Chang, P.S., Wilkerson, J., Marks, F., Black, P.G., 1999. Revised ocean backscatter models at C and Ku-band under high-wind conditions. J. Geophys. Res. 104, 11485–11497.

Drennan, W.M., Donelan, M.A., Terray, E.A., Katsaros, K.B., 1996. Oceanic turbulence dissipation measurements in SWADE. J. Phys. Oceanogr. 26, 808–815.

Fairall, C.W., Hare, J.E., Edson, J.B., McGillis, W., 2000. Parameterization and micrometeorological measurements of air–sea gas transfer. Boundary - Layer Meteorol. 96, 63–105.

Frew, N.M., Bock, E.J., McGIllis, W.R., Karachintsev, A.V., Hara, T., Muensterer, T., Jaehne, B., 1995. Variation of air–water gas transfer with wind stress and surface viscoelasticity. In: Jaehne, B., Monahan, E.C. (Eds.), Air–Water Gas Transfer, pp. 529–541.

Garbe, C.S.., Jaehne, B., Haussecker, H., 2001. Measuring sea surface heat flux and probability distribution of surface renewal events. In: Saltzman, E.S., Donelan, M., Drennan, W., Wanninkhof, R. (Eds.), AGU Monograph Gas Transfer at Water Surfaces, pp. 109–114.

Gemmrich, J.R., Farmer, D.M., 1999. Observations of the scale and oc-currence of breaking surface waves. J. Phys. Oceanogr. 29, 2595–2606.

Hare, J.E., Fairall, C.W., McGillis, W.R., Edson, J.B., Ward, B., Wanninkhof, R., 2004. Evaluation of the National Oceanic and Atmospheric Administration/Coupled-Ocean Atmospheric Response Experiment (NOAA/COARE) air–sea gas transfer parameterization using GasEx data. J. Geophys. Res. 109, C08S11. doi:10.1029/2003JC001831.

Jaehne, B., Muennich, K.O., Rosinger, R., Dutzi, A., Huber, W., Libner, P., 1987. On the parameterization of air–water gas exchange. J. Geophys. Res. 92, 1937–1949.

Jo, Y.-H., Yan, X.-H., Pan, J., Liu, W.T., 2004. Sensible and latent heat flux in the tropical pacific from satellite multi-sensor data. Remote Sens. Environ. 90, 166–177.

Johnes, C.H., Gautler, C., Thimothy Liu, W., 2001. Satellite observations of latent and sensible heart fluxes in the tropical Pacific Ocean. WCRP/SCOR Workshop on Intercomparison and Validation of Ocean-Atmosphere Flux Fields, May 21–24, 2001, Bolger Center, Potomac, MD, pp. 14–19.

Katsaros, K.B., Liu, W.T., Businger, J.A., Tillman, J.E., 1977. Heat transport and thermal structure in the interfacial boundary layer measured in an open tank of water in turbulent free convection. J. Fluid Mech. 83, 311–335.

Kitaigorodskii, S.A., Donelan, M.A., 1984. Wind-wave effects on gas transfer. In: Brutseart, W., Jirka, G.H. (Eds.), Gas Transfer at the Water Surfaces. Reidel, pp. 147–170.

Kitaigorodskii, S.A., Donelan, M.A., Lumley, J.L., Terray, E.A., 1983. Wave-turbulence interactions in the upper ocean: Part II. J. Phys. Oceanogr. 13, 1988–1999.

Komen, G.J., Cavaleri, L., Donelan, M., Hasselmann, K., Hasselmann, S., Janssen, P.A.E.M., 1994. Dynamics and Modelling of Ocean Waves. Cambridge University Press. 532 pp.

Liss, P.S., Merlivat, L., 1986. Air–sea gas exchange rates: introduction and synthesis. In: Buat-Menard, P. (Ed.), The Role of Air–Sea Exchange in Geochemical Cycling. D.Reidel, pp. 113–127.

Mellor, G.L., Yamada, T., 1982. Development of a turbulence closure model for geophysical fluid problems. Rev. Geophys. 20, 851–875.

Monahan, E.C., Lu, M., 1990. Acoustically relevant bubble assemblages and their dependence on meteorological parameters. IEEE J. Oceanic Eng. 15, 340–349.

Monahan, E.C., O'Muircheartaigh, I., 1980. Optimal power-law description of oceanic whitecap coverage dependence on wind speed. J. Phys. Oceanogr. 10, 2094–2099.

Monahan, E.C., Fairall, C.W., Davidson, K.L., Boyle, B.J., 1983. Observed inter-relation between 10-m winds, ocean whitecaps and marine aerosols. Q. J. R. Meteorol. Soc. 109, 379–392.

Nightingale, P.D., Malin, G., Law, C.S., Watson, A.J., Liss, P.S., Liddicoat, M.I., Boutin, J., Upstill-Goddard, R.C., 2000. In situ evaluation of air–sea gas exchange parameterizations using novel conservative and volatile tracers. Glob. Biogeochem. Cycles 14, 373–387.

Oakey, N.S., 1985. Statistics of mixing parameters in the upper ocean during JASIN phase 2. J. Phys. Oceanogr. 15, 1662–1675.

Pan, Jiayi, Yan, Xiao-Hai, Jo, Young-Heon, Zheng, Quanan, Liu, W. Timothy, 2004. A new method for estimation of the sensible heat flux under unstable conditions using satellite vector winds. J. Phys. Oceanogr. 34, 968–977.

Pinker, R.T., Katsaros, K.B., Zhang, B., 2001. Prospects for satellite estimates of net air–sea flux. WCRP/SCOR Workshop on Intercomparison and Validation of Ocean-Atmosphere Flux Fields, May 21–24, 2001, Bolger Center, Potomac, MD, pp. 28–31.

Rascle, N., Ardhuin, F., Terray, E.A., 2006. Drift and mixing under the ocean surface. Part 1: A coherent one-dimensional description with application to unstratified conditions. J. Geophys. Res. 111, C03016. doi:10.1029/2005JC003004.

Saunders, P.M., 1967. The temperature at the ocean–air interface. J. Atmos. Sci. 24, 269–273.

Schlüssel, P., Soloviev, A., 2001. Air–sea gas exchange: cool skin and gas transfer velocity in the North Atlantic Ocean during GasEx-98. Adv. Space Res. 29 (1), 107–110.

Schlüssel, P., Schanz, L., Englisch, G., 1995. Retrieval of latent heat flux and longwave irradiance at the sea surface from SSM/I and AVHRR measurements. Adv. Space Res. 16 (10), 107–116.

Schulz, J., Meywerk, J., Ewald, S., Schlüssel, P., 1996. Evaluation of satellite-derived latent heat fluxes. J. Climate 10, 2782–2795.

Soloviev, A.V., 2007. Coupled Renewal Model of Ocean Viscous Sublayer, Thermal Skin Effect and Interfacial Gas Transfer Velocity.

Journal of Marine Systems (Elsevier) 66, 19–27 (this issue). doi:10.1016/j.jmarsys.2006.03.024.

Soloviev, A., Lukas, R., 2003. Observation of wave enhanced turbulence in the near-surface layer of the ocean during TOGA COARE. Deep-Sea Res., Part 1, Oceanogr. Res. Pap. 50, 371–395.

Soloviev, A., Lukas, R., 2006. The Near-Surface Layer of the Ocean: Structure, Dynamics, and Applications. Springer, 572 pp.

Soloviev, A.V., Schlüssel, P., 1994. Parameterization of the cool skin of the ocean and of the air–ocean gas transfer on the basis of modeling surface renewal. J. Phys. Oceanogr. 24, 1339–1346 and 1965.

Soloviev, A.V., Schlüssel, P., 1996. Evolution of cool skin and direct air–sea gas transfer coefficient during daytime. Boundary - Layer Meteorol. 77, 45–68.

Soloviev, A.V., Schlüssel, P., 2002. A model of the air–sea gas exchange incorporating the physics of turbulent boundary layer and the properties of sea surface. In: Saltzman, E.S., Donelan, M., Drennan, W., Wanninkhof, R. (Eds.), AGU Monograph Series Gas Transfer at Water Surfaces, pp. 141–146.

Soloviev, A.V., Vershinsky, N.V., Bezverchnii, V.A., 1988. Small-scale turbulence measurements in the thin surface layer of the ocean. Deep-Sea Res. 35, 1859–1874.

Tans, P.P., Fung, I.Y., Takahashi, T., 1990. Observational constraints on the global atmospheric CO_2 budget. Science 247, 1431–1438.

Terray, E.A., Donelan, M.A., Agrawal, Y.C., Drennan, W.M., Kahma, K.K., Williams III, A.J., Hwang, P.A., Kitaigorodskii, S.A., 1996. Estimates of kinetic energy dissipation under breaking waves. J. Phys. Oceanogr. 26, 792–807.

Thorpe, Woolf, 1991. Bubbles and the air–sea exchange of gases in near-saturation conditions. J. Mar. Res. 49, 435–466.

Thorpe, S.A., Jackson, J.F.E., Hall, A.J., Lueck, R.G., 2003. Measurements of turbulence in the upper ocean mixing layer using Autosub. J. Phys. Oceanogr. 33, 122–145.

Toba, Y., 1972. Local balance in the air–sea boundary process, I. On the growth process of wind waves. J. Oceanogr. Soc. Jpn 28, 109–121.

Wang, Q., Monahan, E.C., Asher, W.E., Smith, P.M., 1995. Correlation of whitecap coverage and gas transfer velocity with microwave brightness temperature for plunging and spilling breaking waves. In: Jaehne, B., Monahan, E.C. (Eds.), Air–Water Gas Transfer. AEON Verlag & Studio, 63454 Hanau, pp. 217–225.

Wanninkhof, R., 1992. Relationship between wind speed and gas exchange over the ocean. J. Geophys. Res. 97, 7373–7382.

Wanninkhof, R., McGillis, W.R., 1999. A cubic relationship between air–sea CO_2 exchange and wind speed. Geophys. Res. Lett. 26 (134), 1889–1892.

Wanninkhof, R.H., Doney, S., Peng, T.-H., Bullister, J.L., Lee, K., Feely, R.A., 1999. Comparison of methods to determine the anthropogenic CO_2 invasion into the Atlantic Ocean. Tellus 51B, 511–530.

Ward, B., Donelan, M.A., 2006. Thermometric Measurements of the Molecular Sublayer at the Water Surface in a Wind-Wave Tank. Geophys. Res. Lett. 33, L07605. doi:10.1029/2005GL024769.

Woolf, D.K., 1995. Energy dissipation through wave breaking and the air–sea gas exchange of gases. In: Jaehne, B., Monahan, E.C. (Eds.), Air–Water Gas Transfer. AEON Verlag & Studio, 63454 Hanau, pp. 185–195.

Woolf, D.K., 1997. Bubbles and their role in gas exchange. In: Liss, Peter S., Duce, Robert A. (Eds.), The Sea Surface and Global Change. Cambridge University Press, Cambridge, UK, pp. 173–206.

Woolf, D.K., 2005. Parameterizations of gas transfer velocities and sea-state-dependent wave breaking. Tellus 57B, 87–94.

Zhang, X., Harrison, S., 2004. A laboratory observation of the surface temperature and velocity distributions on a wavy and windy air–sea interafce. Phys. Fluids 16 (8), L1–L8.

Zhao, D., Toba, Y., 2001. Dependence of whitecap coverage on wind and wind-wave properties. J. Oceanogr. 57, 603–616.

Zhao, D., Toba, Y., Suzuki, Y., Komori, S., 2003. Effect of wind waves on air–sea gas exchange: proposal of an overall CO_2 transfer velocity formula as a function of breaking-wave parameter. Tellus 55B, 478–487.